XPS and AFM-IR correlative analysis of a ziggurat-structured ZDDP tribofilm

Stuart Lyon (stuart.lyon@manchester.ac.uk)
Manchester University https://orcid.org/0000-0002-3320-1066
Kostas Despotelis
National Physical Laboratory
Suzanne Morsch
University of Manchester
Ben Spencer
University of Manchester

Article

Keywords: ZDDP, Tribofilm, XPS, AFM-IR

Posted Date: May 18th, 2022

DOI: https://doi.org/10.21203/rs.3.rs-1639167/v1

Abstract

Dynamic single asperity contact, using Atomic Force Microscope (AFM) probe tips, have been recently shown to be a powerful tool for investigating the tribological properties of surfaces. Here, we demonstrate a novel in-situ approach that produces a multilayer, ziggurat-structured, tribofilm developed over time. On a single sample produced during one uninterrupted experiment, each distinct layer uniquely represents a different stage of tribofilm development arising from decomposition of zinc dialkyl-dithiophosphate (ZDDP). We were able to successfully analyse the structure of the most developed inner layers, which reached a thickness of more than 130 nm, and the less developed outer regions, which were just a few nm thick, as well as intermediate layers. Thus, selected area X-ray photoelectron spectroscopy, measured a shift in the composition of zinc, sulphur and phosphorus, and a decrease in the sulphide:sulphate and ZnS:ZnO ratios as the film developed. Furthermore, AFM-IR, used in this application for the first time, directly identified S = O groups in the early stage of tribofilm growth as well as in the thermofilm. However, during later stages of growth, and particularly in the most developed central layers of the 'ziggurat', structure (poly)phosphates were detected (P = O, P-O-P, P-O-C). This confirms the previously suspected changes in the chemistry of such tribofilms as they develop.

Introduction

Zinc di-thiophosphates (ZDDPs) began to be incorporated as additives into lubrication oils, to protect component parts under conditions of enhanced wear, in the 1940s after patents were first issued to the Lubri-zol Corporation [1]. Some eighty years' later, as pointed out by Spikes [2], they remain: "*the most successful lubricant additives ever invented*". The utility of ZDDPs lie in their ability to simultaneously function as anti-wear agents, mild extreme-pressure agents, and as oxidation and corrosion inhibitors. Furthermore, this performance is delivered at low cost in comparison with alternative chemistries meaning that ZDDP continues to be included in practically all engine oils.

Morphologically, ZDDP tribological anti-wear films do not always appear to form as continuous films. Rather, as noted by Sheasby et al. [3], Aktary et al. [4], and others, they can initiate and subsequently develop as a matrix of discontinuous raised islands. Sliding wear promotes the formation of ZDDP tribofilms at considerably lower temperatures than are required for thermal film formation. A common explanation, that decomposition of the ZDDP molecule is due to transient energy dissipation / heating during asperity contact, is unlikely. A more credible mechanism, proposed and largely confirmed by Zhang and Spikes [5], is that the local applied shear stress in the fluid generated during rubbing contact results in a significant reduction of the activation energy for ZDDP decomposition. Thus, tribofilm formation is essentially a chemo-mechanical phenomenon.

ZDDPs are susceptible to thermally activated [6] and tribologically enhanced [7] decomposition forming relatively volatile species (e.g. alkyl sulfides, H_2S, etc.) and leaving an amorphous solid and adherent residue. Using sulfur and phosphorus radiotracers, Loesler et al. established that under practical engine conditions ZDDP tribofilms were around 100 nm in thickness and in dynamic equilibrium between

formation (due to decomposition of the ZDDP molecule) and removal (due to abrasive rubbing) [7]. In a later paper the same authors confirmed that the film was phosphorus-rich with a phosphorus-to-sulfur ratio in the tribofilm significantly greater than in the molecule [8]. ZDDPs therefore decompose to form protective layers against wear due to temperature and frictional processes forming, respectively, a thermal film or a tribofilm. These general findings have been confirmed and further refined many times using multiple approaches. For example, Bancroft et al. used x-ray absorption near-edge structure (XANES) analysis to show that thermal films and tribofilms appear to have similar chemistry (i.e. contain polyphosphate species) and are robust mechanically (adherent, coherent and resistant to rubbing) [9]. Martin considered the acid-base chemistry of ZDDP and deduced that a dual layer structure was present with a sulfide-rich surface on the iron substrate covered by a phosphate-rich layer acting as the main anti-wear component [10] and confirmed by XANES subsequently [11]. Piras et al. [12] used correlative vibrational spectroscopy (FTIR) with x-ray photoelectron spectroscopy (XPS) to confirm the presence of POO^{-}, P-O-P, P-O and P = O (corresponding to inorganic phosphate and its molecular precursors) and a metallic sulfide species in agreement with Martin's model. Recently Neville's group performed *in-situ* x-ray absorption spectroscopy (XAS) using synchrotron radiation on "ashless" DDP (i.e. identical chemistry but without zinc) [13]. This demonstrated initial formation of iron sulfate, reducing to iron sulfide, followed by the development of iron phosphates that eventually link to form longer chain polyphosphate structures as the tribofilm thickens. The overwhelming evidence is, therefore, that ZDDP tribofilms comprise a physically inhomogeneous structure in the plane of the substrate that is also chemically segregated perpendicular to the substrate. Metallic sulphides are present at the film/substrate interface and these transition to a metallic phosphate/polyphosphate that forms the bulk of the film.

Although true *in-operando* analysis of tribofilm formation remains challenging it has become possible with the advent of fluid cells in atomic force microscopy (AFM). First demonstrated by Govsami et al. [14], under these conditions a tribofilm develops at the single-point asperity formed by the AFM tip during sliding. Variation of applied force and translation speed at the AFM tip allows a tribofilm to be built up layer-by-layer giving direct *in-situ* measurement of film growth rate and morphology [15]. In this contribution we uniquely develop a stepped pyramid structure, or ziggurat, using AFM single asperity growth such that both early and later stages of tribofilm formation can be analysed on the same sample. We then use XPS and sub-diffraction vibrational spectroscopy (AFM-IR) to analyse the different stages of film growth on each ziggurat step.

Experimental Methods

Tribofilm development

Substrates for tribofilm formation were prepared from commercial, polished silicon wafers (IDB Technologies Ltd., UK), that were ultrasonically cleaned for 10 min in ethanol + acetone. The wafer was then vacuum sputter coated (150T Plus, Quorum Technologies, UK) initially with 3 nm of 99.9% Cr as an adhesion layer, followed with 10 nm of 99.9% Fe comprising the model metallic substrate. The lubricant

formulation used 99 wt.% base-stock oil (classified as petroleum distillate, hydrotreated heavy paraffinic group III, with a kinematic viscosity of 4 $mm^2 s^{-1}$ at 100°C). To this was added the anti-wear additive: 1 wt.% of mixed primary and secondary zinc di-alkyl di-thiophosphate (ZDDP) characterized by a kinematic viscosity of 6–14 $mm^2 s^{-1}$ at 100°C containing phosphorus of approximately 0.8 wt.% and zinc content of 0.9 wt.%. This resulted in approximate concentrations of 800 ppm phosphorus and 900 ppm zinc, respectively, in the finished formulated oil.

ZDDP tribofilms were generated in-situ with an atomic force microscope (Dimension Icon 3100, Bruker), using a single asperity contact between the AFM probe tip and the substrate. Diamond like carbon (DLC) coated cantilevers with a tip radius < 15 nm and a general half-cone angle of ~ 25 ° falling to ~ 10 ° at the apex were selected due to their high resistance to wear (Multi75DLC, Innovative Solutions, Bulgaria). Calibration of the cantilever spring constant (nominally 1–7 $N m^{-1}$) was performed using the “thermal tune” method of Torii et al. [6] while deflection sensitivity (D_{sens}, $m V^{-1}$) was determined from the deflection error (in nm) versus tip displacement (in nm) curve, obtained from an approach and retract ramp of the tip onto the sample according to the method of Hutter and Beckhoefer [17]. These processes were largely automated by the Bruker instruments software. The applied normal force (F) on the cantilever was determined by multiplying the deflection set point value (D_{sp}, V), the experimentally calculated cantilever spring constant (k, $N m^{-1}$), and the experimentally determined deflection sensitivity. This gave a calculated Hertzian contact pressure at the AFM cantilever tip of 5.5 GPa.

AFM fluid cells equipped O-ring seals are often subject to leakage around the seal however, here we use a novel design by Bruker, Fig. 1, whereby the droplet is confined between the substrate and tip holder thus achieving a stable meniscus without the need for a seal. Since the stability of the fluid meniscus is effectively limited by evaporation at the meniscus edge, large numbers of tribo-cycles can be studied in experiments lasting tens of hours. Control experiments conducted at room temperatures resulted in no tribofilm growth but did result in observable wear/polishing of the substrate. However, a tribofilm was readily formed when the substrate was maintained at 100 ± 1°C indicating that an elevated temperature was needed for film formation.

Originally, we planned to generate tribo-films at different locations on a single iron-coated silicon substrate using common sliding conditions but for varying times which would simplify analyses. However, on one occasion the probe tip was inadvertently not moved when a larger scan area was chosen. Subsequent AFM topographic analysis showed development of new film not only on the fresh larger area adjacent to the original locus but also on top of the original film, a phenomenon that was not expected and, we believe, not reported to date. After confirming multiple times that this process was repeatable, we undertook to analyse the tribofilm on a single sample formed as a ziggurat (or stepped pyramid) where each layer comprised a different stage in time of tribofilm growth. The multilayer structure was generated by changing the scan area and the number of sliding cycles at a fixed scanning frequency of 40 Hz and AFM tip pressure of 5.5 GPa. As the scanned area was increased stepwise the scanning speed changed from 126 $\mu m s^{-1}$ for the 2 x 2 μm first layer and up to 1628 $\mu m s^{-1}$ for the final

20 x 20 μm layer. We appreciate that this results in a different sliding speed for each new layer, but this constraint was imposed to complete experiments in a reasonable time frame. Image scans are presented with a resolution of 256 x 256 pixels.

Analytical techniques

Prior to analysis the tribofilm structure was rinsed with n-pentane to remove excess ZDDP from the surface. Imaging was performed using a field emission scanning electron microscope (FEI Quanta 650) equipped with an energy dispersive x-ray spectrometer at an incident beam energy of 15 keV resulting in an interaction depth of around 1 μm. Surface sensitive (sampling depth 3–10 nm) X-ray electron spectroscopy used a Kratos Axis Ultra Hybrid XPS equipped with an Al Kα mono-chromated X-ray source (1486.6 eV, 10 mA emission at 150 W). The sampled area was controlled using apertures with sampling areas of 27 x 27 μm, 55 x 55 μm and 300 x 700 μm covering both the thermal film and the tribofilm. Survey spectra were recorded with an analyser pass energy of 80 eV, and high-resolution spectra with a pass energy of 20 eV. Peak fitting and quantification was undertaken using the CASAXPS software with binding energies referred to C_{1s} at 284.8 eV.

Nanoscale infrared analysis (AFM-IR) was performed using a NanoIR2 system (Anasys Instruments, Santa Barbara) operating with top-down illumination. During AFM-IR analysis, specimens are illuminated by a pulsed, tuneable infrared source (optical parametric oscillator, 10 ns pulses at a repetition rate of 1 kHz, approximate beam spot size 30 μm). IR absorbance is detected by deflection of an AFM probe tip in contact with the surface which defines in our case an analytical area of ~ 150 x 150 nm well above the resolution limit of 50 x 50 nm. Spectra were obtained with the AFM probe tip in contact with the sample surface while stepping the pulsed infrared source through the wavelengths of the spectral region and recording the deflection response. AFM-IR spectral peaks and intensities gathered in this way correlate well with infrared absorbance measured using conventional macroscopic FTIR (e.g. for amorphous polyphosphate films [18]) and, with spectral averaging, sufficient sensitivity has been demonstrated for the local characterisation of functionalised graphene oxide flakes [19].

Results

Tribofilm development

Stepped pyramids (ziggurats) were constructed using continuous fluid cell experiments lasting several days. During this time the scanned area was increased stepwise so that the previously developed tribofilm was included within the new scan region and thus continued to develop under the applied sliding load. Intermittently, the structure was imaged in contact mode with a non-perturbative load. The number of tribo-cycles selected for each step was limited due to operational (the fluid meniscus occasionally collapsed at unpredictable moments) and time constraints. Thus, scans were set running as early as possible in a morning and the scan areas changed 3–6 hours later (prior to evening departure) and again 18–19 hours later (after morning arrival), etc. In this paper we describe the production and analysis of a 4-stage stepped tribofilm which is typical of those that can be formed using this procedure.

An initial tribofilm was formed by sliding the AFM at a load corresponding to a tip pressure of ~ 5.5 GPa over an area of 2 x 2 μm for 1000 cycles at 40 Hz. After the scan had finished, the area was increased to 4 x 4 μm and a 3D topographic image was obtained using imaging parameters, Fig. 2(a). Next, the AFM tip load and scan rate were returned to tribofilm formation conditions over the same 4 x 4 μm region (i.e. inclusive of the initial 2 x 2 μm area of stage 1 growth) for a further 10,500 cycles. The film was then revealed under imaging conditions over a larger 8 x 8 μm area, Fig. 2(b). Repeating the same process, the imaged 8 x 8 μm area became the locus for formation of the third tribofilm layer for an additional 3000 cycles. Afterwards imaging of a larger 20 x 20 μm area reveals a stepped pyramid (ziggurat) morphology, Fig. 2(c). Finally, after an additional 10,000 cycles, the completed tribofilm was visualised over an area of 40 x 40 μm, Fig. 2(d).

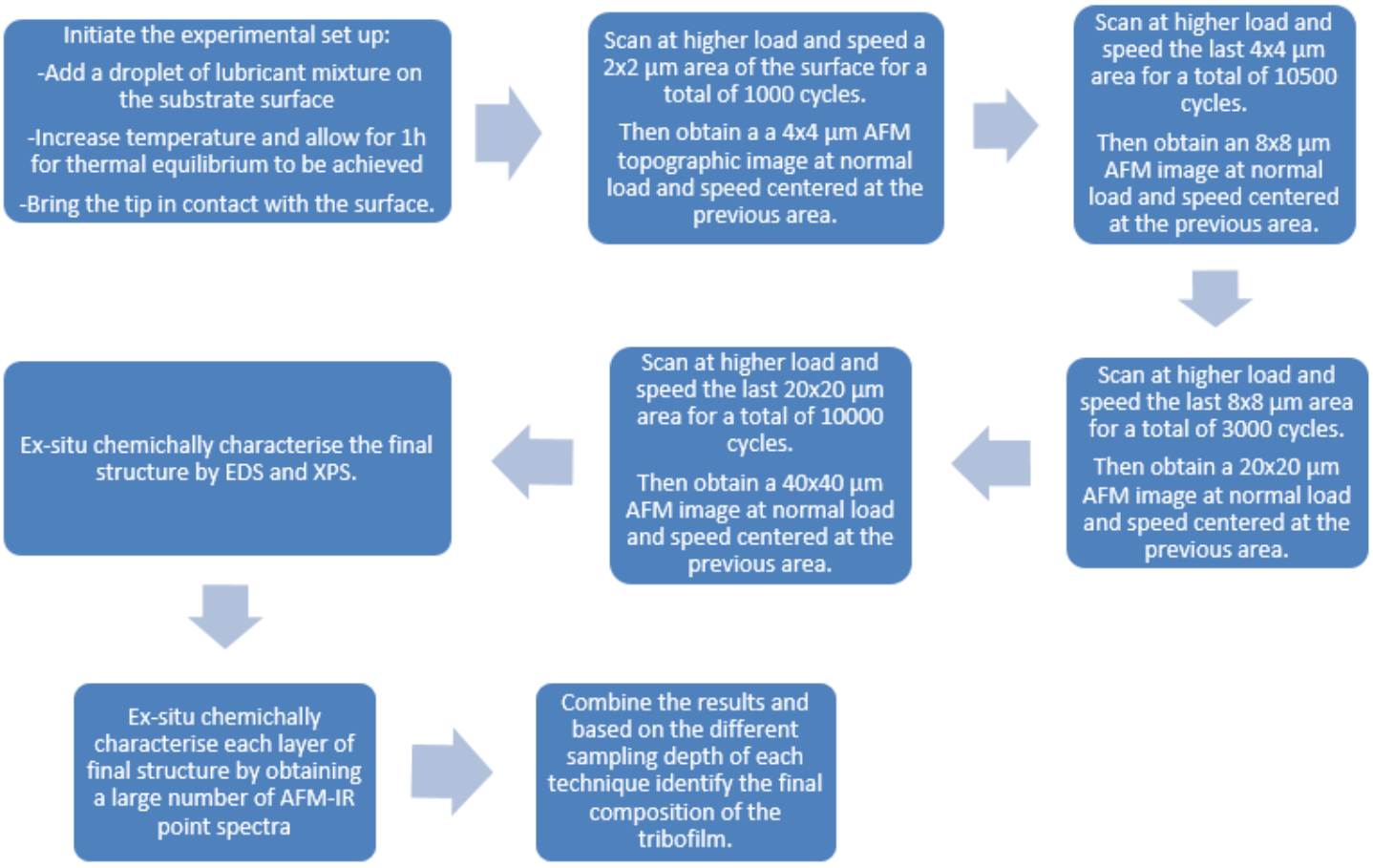

Table 1 Workflow scheme for the single-point AFM sliding tribological experiments.

Table 1: XPS elemental analyses and analytical ratios for Zn_{2p}, S_{2p} and P_{2p} over increasing areas of the early tribofilm

Analytical area	*Tribofilm area*	P_{2p}	S_{2p}	Zn_{2p}	*Zn/P*	*Zn/S*	*P/S*
700 x 300 µm	0.2%	0.78%	1.83%	1.59%	2.04	0.87	0.43
55 x 55 µm	13%	0.82%	1.75%	1.42%	1.72	0.81	0.47
27 x 27 µm	54%	0.93%	1.35%	1.14%	1.23	0.84	0.69
Extrapolated	100%	1.05%	0.95%	0.78%	0.74	0.82	1.11

Analytical microscopy

The tribofilm initially generated after 1000 cycles over 4 μm^2 appears rough with peak film thickness around 30 nm. Expanding the area to 16 μm^2, and after a total of 11,500 cycles, the tribofilm has grown into a relatively homogenous layer around 100 nm in total thickness. At this stage there is no evident separation between the first and second growth stages although the layer has been smeared in the direction of the AFM tip travel (right-to-left). After a further 3,000 cycles over 64 μm^2 (14,500 in all) a smooth shelf has clearly developed with thickness around 16 nm and a peak thickness of 105 nm. Finally, an additional 10,000 cycles (now totalling 24,500) over 400 μm^2 results in the formation of a second shelf of thickness around 20 nm and a total thickness of 130 nm. We note that the maximum thickness of the tribofilm steadily increased at each stage showing that equilibrium between film removal and regeneration had not yet been reached. The layer thicknesses were determined from the 2D topographic cross-sections shown in Fig. 3.

Figure 4(a) shows an optical microscope image of the 20 x 20 µm multi-layer tribofilm structure and Fig. 4(b) the corresponding secondary electron image. In both cases the different layers can easily be distinguished. Figures 4(c) to (h) show energy dispersive x-ray spectroscopy (EDS) elemental maps where attenuation of the silicon signal, due to its relatively low energy X-ray (1.74 keV), is a proxy indicator for the tribofilm thickness. In contrast the zinc, phosphorus, sulfur and oxygen signals increase in line with tribofilm thickness. Finally, the EDS map for iron is relatively homogeneous across the tribofilm region due its more energetic X-ray (7.11 keV) that can escape from greater depth.

XPS surface analysis

The ziggurat tribofilm consists of 2 merged layers (4 x 4 µm) with a 3rd layer (8 x 8 µm) and a 4th layer (20 x 20 µm). Consequently the 4th layer forms 86% while the 3rd and 4th layers together form 96% of the total tribofilm area. Thus, XPS analysis that extends beyond the confines of the film will be dominated by contributions from the 4th and 3rd layers which represent tribofilm compositions at an early stage of film growth.

Figure 5 presents high resolution XPS spectra for the elements of interest (Zn_{2p}, S_{2p} and P_{2p}) in the tribofilm obtained by sampling three areas centred on the tribofilm. For the largest sampling area, 700 x

300 µm, the measurement is dominated by the thermo-film on the surrounding substrate. However, spectra recorded from 55 x 55 µm and 27 x 27 µm include increasing contributions from the tribofilm. The elemental composition within each of the three areas is presented in Table 2 and have been linearly extrapolated to estimate the composition of the early tribofilm. The analytical peaks for Zn *2p*, S *2p* and P *2p* appear at the same binding energies, with differences in intensity reflected changes in the local chemical composition. As the analysis area shrinks from the thermo-film onto the tribofilm, the zinc to sulfur remains approximately constant, the zinc to phosphorus ratio decreases and the phosphorus to sulfur ratio increases.

Table 2: High resolution XPS analyses of S_{2p} and Zn_{2p} over increasing areas of the early tribofilm

Analytical area	*Tribofilm area*	*S_{2p} - sulfide %*	*S_{2p} - sulfate %*	*Zn_{2p} - ZnS %*	*Zn_{2p} - ZnO %*
700 x 300 µm	0.2%	70.8%	29.2%	79.7%	20.3%
55 x 55 µm	13%	77.2%	22.8%	84.0%	16.1%
27 x 27 µm	54%	82.4%	17.6%	91.9%	8.1%
Extrapolated	100%	91.6%	8.5%	101%	0%

The P $2p_{3/2}$ binding energy appears at around 133.9 eV indicating the presence of phosphate species [20]. The S $2p_{3/2}$ binding energies appear at 162.8 eV and 168.8 eV and can be assigned, respectively, to sulfide [21] and sulfate [22]. The Zn $2p_{3/2}$ binding energy appears at ~ 1020.5 eV and 1022.0 eV and is attributed to the contributions of ZnO [23] and ZnS [24] compounds respectively. Based on these analyses and peak fitting of the high resolution XPS spectra shown in Fig. 9, the changes in the ratio of sulphide/sulphate and ZnS/ZnO ratios were calculated for the three sampling areas (and extrapolated to 100% tribofilm) and are presented in Table 3. The thermofilm is clearly more oxidised than the tribofilm as most sulfate is in the thermofilm. Oxidised zinc (i.e. ZnO) decreases to around zero in the tribofilm while ZnS increases to around 100%. This is because the tribofilm surface is continuously generated, but the thermofilm develops in a constant oxidative state due to the thermal decomposition of the ZDDP additive.

Vibrational spectroscopy

The AFM-IR analytical positions on the stepped tribofilm are indicated in Fig. 6 and the resulting absorption spectra, averaged to reduce background noise, are shown in Fig. 7 (900–1800 cm^{-1}) and Fig. 8 (2600–3700 cm^{-1}). The 3rd (30 nm thick) and 4th layers (15 nm thick) comprise chemistries from the early period of tribofilm growth. These thinner films (and the tribofilm) are dominated by a broad band centred at ~ 1110 cm^{-1}, which shifts up in wavenumber as the tribofilm thickens. This band we assign to

sulfate on the basis of strong S = O absorptions around 1100 cm^{-1} [25] and consistency with the XPS observation that sulfate decreases significantly in thicker films. We discount Piras' suggestion [26] that adsorption in this region is related to phosphorus as the band lies outside both P = O (1320 – 1140 cm^{-1}) and P-O (950–1060 cm^{-1}). However, the shoulder at lower wavenumber (~ 1070 cm^{-1}) becomes stronger as the film thickens and we believe this represents the developing phosphate layer.

The merged 1st and 2nd layers of the tribofilm are thicker (50–120 nm) and comprise the most developed film chemistry. The S = O absorbance at 1110 cm^{-1} is less prominent while the band at ~ 1220 cm^{-1} can be assigned to P = O with P-O appearing at 1070 and 1020 cm^{-1}. Stretching vibrations of P-O-C and P-O-P are at 968 cm^{-1} and 928 cm^{-1} and correspond to proposed polyphosphate chains in the tribofilm volume. This is consistent with XPS results, which showed an increase in phosphorus as the tribofilm develops. It also fits with Zhang and Spikes' model [4] where, under sliding conditions, sulphur initially binds to the surface before a Zn and P rich tribofilm layer develops. Finally, the bands at 1712 cm^{-1} and 1596 cm^{-1} detected in the thickest first and second layers, are characteristic of carbonyl (C = O) and alkene (C = C) respectively.

In the upper AFM-IR spectral range (2600–3700 cm^{-1}) spectra are similar across the different layers in the structure. In all cases, the C-H stretch of an alkene can be identified between 3072 and 3140 cm^{-1} and symmetric and an asymmetric CH_2/CH_3 stretching was assigned to absorbance around 2960 cm^{-1} and 2870 cm^{-1} respectively. The broad absorption peak between 3200 and 3650 cm^{-1} is due to OH stretch. Finally, the stretching vibration observed at around 2784 cm^{-1} gradually intensifies from the thermo-film towards the centre of the structure and appears in combination with the C = O bond in the lower range of the spectrum, therefore could be assigned to a H-(C = O) of an aldehyde.

Compositional variation in the ZDDP tribofilm

We observe a two-layer compositionally varied tribofilm (Fig. 9) where the thermal film and early stage tribofilm (< 15 nm thick) is partially oxidised and contains zinc sulfide, zinc sulfate and zinc oxide with limited amounts of phosphorus. However, as the tribofilm grows beyond 30 nm, phosphate / polyphosphate begins to form the bulk of the film while oxidised zinc and sulfate species are substituted by zinc sulfide.

Conclusions

1. A 4-layered pyramid (ziggurat) tribofilm structure was developed using single-point asperity sliding wear in an AFM over several days growing to ~ 130 nm after 26,000 cycles. The highest layers of the ziggurat correspond to the latter stages of tribofilm growth while the lower layers correspond to early film growth. Thus, all stages of film growth can be examined on a single specimen
2. XPS analysis shows that, compared to the thermal film, phosphorus increases as the tribofilm develops while the zinc-to-sulphur ratio remains largely constant. Zinc sulfate and oxide in the thermofilm and the early tribofilm but only zinc sulfide was found in the thicker tribofilm

3. AFM-IR on individual layers revealed that the S = O species was present predominantly in the thermofilm and early tribofilm. However, a critical shift in film chemistry occurred when the tribofilm was less than 30 nm in thickness with a large reduction in S = O and the appearance of P = O, P-O-P, P-O-C confirming the development of (poly) phosphates during later tribofilm development.

Declarations

Acknowledgments

The authors acknowledge the financial support of BP and the International Centre for Advanced Materials (ICAM). Chris Warrens provided industrial oversight of the project and Laura Felisari supported the experimental work (BP Technology Centre, Pangbourne, UK).

Data availability

Figures 1 and 9 are sketches and contain no data. Figures 2-8 comprise raw image data derived directly from the relevant analytical instrument or microscope. High resolution XPS analyses in Tables 1 and 2 are derived from Figure 5. The corresponding author should be contacted for any further details.

Competing interests

The authors declare no competing financial or non-financial interests

Author contributions

Kostas Despotelis – experimental work and paper preparation; Suzanne Morsch – AFM-IR, editing; Ben Spencer – XPS, editing; Stuart Lyon – project conception, supervision, editing

References

1. Asseff, P.A. US Patent 2261047, Oct 1941.
2. Spikes, H. The history and mechanisms of ZDDP. Tribol. Lett. **17**, (2004) 469–489
3. Sheasby, J.S., T. A. Caughlin, T.A., & Habeeb, J.J. Observation of the antiwear activity of zinc dialkyldithiophosphate additives. Wear, **150** (1991) 247–257
4. Aktary, M., McDermott, M. T. & Torkelson, J. Morphological evolution of films formed from thermooxidative decomposition of ZDDP. Wear **247** (2001) 172–179
5. Zhang, J. and Spikes, H. On the mechanism of ZDDP antiwear film formation. Tribol. Lett. **63**, (2016) 1–15
6. von Luther, H. and Sinha, S.K. Erdol u Kohle-Erdgas-Petrochemie **17** (1964) 91
7. Loesler, E.H. Loeser, R.C. Wiquist and S.B. Twiss, Cam and tappet lubrication: radioactive study of phosphorus in the EP film. ASLE Trans. **1** (1958) 329–335

8. Loesler, E.H. Loeser, R.C. Wiquist and S.B. Twiss, Cam and tappet lubrication: radioactive study of sulfur in the EP film. ASLE Trans. **2** (1958) 199–207
9. Bancroft, G.M., Kasrai, M., Fuller, M., Yin, Y., Mechanisms of tribochemical film formation: stability of tribo- and thermally-generated ZDDP films. Tribology Letters 3 (1997) 47–51
10. Martin, J.M. Antiwear mechanisms of zinc dithiophosphate: a chemical hardness approach, Tribology Letters 6 (1999) 1–8
11. Martin, J. M., Grossiord, C., Le Mogne, T., Bec, S. & Tonck, A. The two-layer structure of Zndtp tribofilms, Part I: AES, XPS and XANES analyses. Tribol. Int. **34** (2001) 523–530
12. Piras, F. M., Rossi, A. & Spencer, N.D. Combined in situ (ATR FT-IR) and ex situ (XPS) study of the ZnDTP-iron surface interaction. Tribology Letters **15** (2003) 181–191
13. Dorgham, A., Parsaeian, P., Azam, A, Wang, C. Ignatyev, K., Mosselmans, F., Morina, A., Neville, A. Tribochemistry evolution of DDP tribofilms over time using in-situ synchrotron XAS. Tribol. Int. **160** (2021) 107026
14. Gosvami, N.N., Bares, J.A., Mangolini, F., Konicek, A.R., Yablon, D.G., Carpick, R.W. Mechanisms of antiwear tribofilm growth revealed in situ by single-asperity sliding contacts. Science **348** (2015) 102–106
15. Liu, X., Tanga, C-Y., Haoa, R., Walsh. K., Zhou, C., Dillon, S.J. Local chemo-mechanical insights into the efficacy of ZDDP additives from in situ single asperity growth and mechanical testing. Tribol. Int. 112, 103–107 (2017)
16. Akihiro Torii, Minoru Sasaki, Kazuhiro Hane and Shigeru Okuma, A method for determining the spring constant of cantilevers for AFM Meas. Sci. Technol. **7**, 179–184 (1996)
17. Hutter, J. L. & Bechhoefer, J. Calibration of Atomic-Force Microscope Tips. Rev. Sci. Instrum. **64**, 1868–1873 (1993)
18. Morsch, S. *et al.* The Unexpected Role of Carbonate Impurities in Polyphosphate Corrosion Inhibition. Sci. Rep. **8**, 2–8 (2018)
19. Bartlam, C. *et al.* Nanoscale infrared identification and mapping of chemical functional groups on graphene. Carbon N. Y. **139**, 317–324 (2018)
20. R. Franke, T. Chasse, P. Streubel, A. Meisel, J. Elect. Spect. Rel. Phen. 56 (1991) 381
21. X.-R Yu, F. Liu, Z.-Y. Wang, Y. Chen, J. Elect. Spect. Rel. Phen. 50 (1990) 159
22. Davide Barreca, Alberto Gasparotto, Cinzia Maragno, et al. Surface Science Spectra 9 (2002) 54
23. B. R Strohmeier and D. M. Hercules, J. Catalysis 86 (1984) 266
24. K. Laajalehto, I. Kartio, P. Nowak. Appl. Surf. Sci. 11 (1994) 11
25. Coates, J. Interpretation of Infrared Spectra, A Practical Approach. Encycl. Anal. Chem. 10815–10837 (2006).
26. Piras, F. M., Rossi, A. & Spencer, N. D. Growth of tribological films: In situ characterization based on attenuated total reflection infrared spectroscopy. Langmuir **18**, 6606–6613 (2002).

Figures

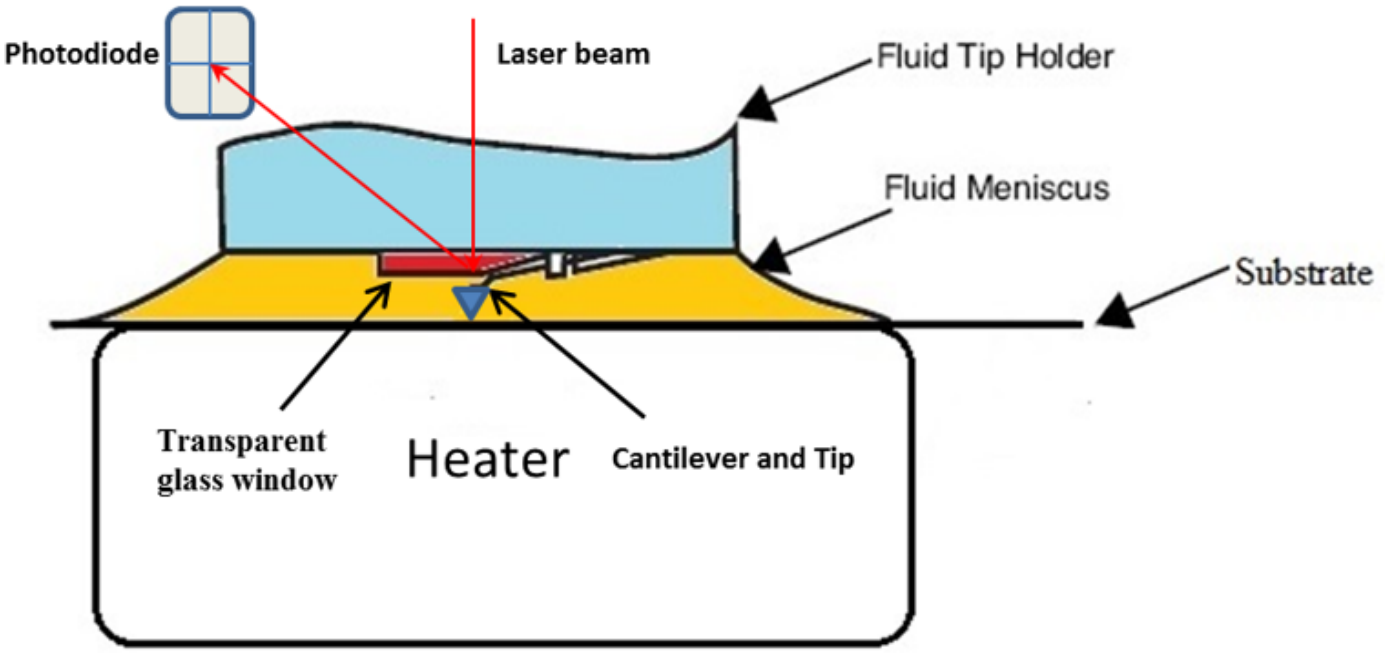

Figure 1

Schematic diagram of the Bruker AFM fluid cell and substrate/heater

Figure 2

See image above for figure legend

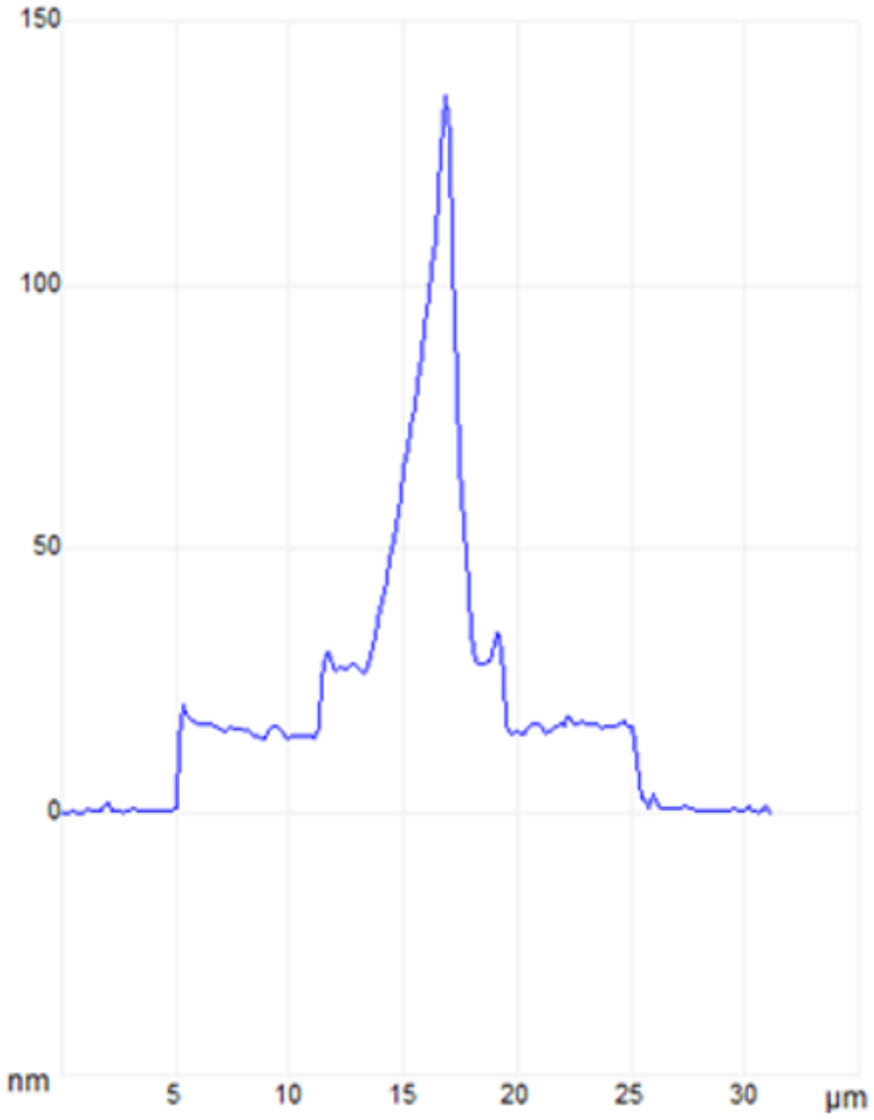

Figure 3

Cross-section of the multilayer tribofilm structure showing the thickness of the various layers

Figure 4

a) Optical microscope and b) secondary electron image of the 20x20µm multi-layer tribofilm structure. EDS elemental maps gathered for (c) sulfur, (d) zinc, (e) phosphorus, (f) silicon (g) oxygen and (h) iron.

Figure 5

High resolution XPS spectra of the Zn *2p*, S *2p* and P *2p* obtained from the sampling areas, with the approximate sampled area presented in the last column right.

Figure 6

AFM-IR 30x30 µm topographic images indicating the analytical locus: [LEFT] grey: thermo-film; blue (outer tribofilm); yellow: central tribofilm; [RIGHT] green (first two tribofilm layers merged together).

Figure 7

AFM-IR spectra (900-1800 cm^{-1}) for each tribo-layer and their assigned peaks.

Figure 8

AFM-IR spectra (2600-3700 cm^{-1}) for each tribo-layer and their assigned peaks.

Figure 9

Sketch of through thickness compositional variation within the ZDDP tribofilm